Conformational Adaptability of Redβ during DNA Annealing and Implications for Its Structural Relationship with Rad52

Axel Erler[1], Susanne Wegmann[2], Celine Elie-Caille[2,3], Charles Richard Bradshaw[4], Marcello Maresca[1], Ralf Seidel[5], Bianca Habermann[4,6], Daniel J. Muller[2]* and A. Francis Stewart[1]*

[1]*Genomics, Biotechnology Center, Technische Universität Dresden, Tatzberg 47–51, 01307 Dresden, Germany*

[2]*Cellular Machines, Biotechnology Center, Technische Universität Dresden, Tatzberg 47–51, 01307 Dresden, Germany*

[3]*FEMTO-ST Institute, UMR 6174 CNRS, CLIPP Platform, 32 Av. Observatoire, 25044 Besançon cedex, France*

[4]*Max Planck Institute of Molecular Cell Biology and Genetics, Pfotenhauerstrasse 108, 01307 Dresden, Germany*

[5]*DNA Motors, Biotechnology Center, Technische Universität Dresden, Tatzberg 47–51, 01307 Dresden, Germany*

[6]*Scionics Computer Innovation GmbH, Tatzberg 47–51, 01307 Dresden, Germany*

Single-strand annealing proteins, such as Redβ from λ phage or eukaryotic Rad52, play roles in homologous recombination. Here, we use atomic force microscopy to examine Redβ quaternary structure and Redβ–DNA complexes. In the absence of DNA, Redβ forms a shallow right-handed helix. The presence of single-stranded DNA (ssDNA) disrupts this structure. Upon addition of a second complementary ssDNA, annealing generates a left-handed helix that incorporates 14 Redβ monomers per helical turn, with each Redβ monomer annealing ≈11 bp of DNA. The smallest stable annealing intermediate requires 20 bp DNA and two Redβ monomers. Hence, we propose that Redβ promotes base pairing by first increasing the number of transient interactions between ssDNAs. Then, annealing is promoted by the binding of a second Redβ monomer, which nucleates the formation of a stable annealing intermediate. Using threading, we identify sequence similarities between the RecT/Redβ and the Rad52 families, which strengthens previous suggestions, based on similarities of their quaternary structures, that they share a common mode of action. Hence, our findings have implications for a common mechanism of DNA annealing mediated by single-strand annealing proteins including Rad52.

© 2009 Elsevier Ltd. All rights reserved.

*Corresponding authors. E-mail addresses: mueller@biotec.tu-dresden.de; stewart@biotec.tu-dresden.de.

Abbreviations used: ssDNA, single-stranded DNA; SSAP, single-strand annealing protein; dsDNA, double-stranded DNA; EM, electron microscopy; AFM, atomic force microscopy.

Introduction

The formation of joint DNA molecules by recombinases is a central step in homologous recombination.[1–4] Two paradigms are known: strand invasion and strand annealing.[5] Strand invasion involves displacement loop formation and DNA-strand exchange, which is catalyzed by DNA-dependent ATPases of the RecA/RAD51 protein family.[6,7] Here, we focus on strand annealing mediated by single-strand annealing proteins (SSAPs), which directly promote annealing of complementary strands. Although strand annealing is the conceptually less complex mechanism, its molecular mechanism remains poorly understood. Protein sequence analysis has defined three SSAP families, named after their preeminent representatives, RecT/Redβ, Erf, and Rad52.[8]

Redβ and RecT are coliphage proteins encoded in operons together with cooperating 5′–3′ exonucleases (Redα and RecE, respectively). The respective exonuclease partners are required to mediate homologous recombination with double-stranded DNA (dsDNA).[9,10] Despite the lack of understanding of the molecular mechanism[9,11] or the role in phage metabolism,[12] homologous recombination mediated by these proteins is a cornerstone of the useful DNA engineering technology termed 'recombineering'.[13–16]

Redβ has been reported to bind single-stranded DNA (ssDNA) but does not appear to bind dsDNA. Upon addition of complementary ssDNA, the stability of the existing Redβ–ssDNA complex is enhanced. Redβ remains bound to the annealed dsDNA and forms a very stable annealing intermediate.[17,18] No Redβ crystal structure is available. However, quaternary structures of Redβ, with and without DNA, have been inferred from electron microscopy (EM), which reported rings in the absence and presence of ssDNA, and a left-handed helical Redβ–DNA complex after annealing. A model that invoked an initiating role for Redβ rings in the formation of annealing intermediates was proposed.[19] However, several parameters, such as the DNA binding capacity per Redβ monomer and the relationship of helical contour length to DNA length, or the quantitative impact of ssDNA binding, remain unknown.

Rad52 is the best-characterized SSAP due to two crystal structures of the highly conserved N-terminal DNA binding domain of human Rad52.[20,21] Both structures revealed a mushroom-shaped undecameric ring with a central hole lined by a β-barrel-like surface (as well as an external groove lined with positive charges) that probably binds the phosphodiester backbone of ssDNA. However, crystal structures of these undecameric rings, which were formed in the absence of DNA, do not provide explanations for the observed variations in Rad52 conformations under different circumstances. For example, full-length Rad52 appears to form heptameric rings in the absence of DNA and large protein–DNA complexes at heteroduplex intermediates.[22,23] Recently, Sak, a prokaryotic Rad52 homolog, has been shown to also form undecameric rings.[24]

Functional relationships between the three SSAP families have been proposed based upon their abilities to form quaternary structures in the absence and presence of DNA. Various ring and polymer conformations have been described for Redβ, RecT, Erf, and Rad52 quaternary structures.[19,22,25,26] However, these structures are quite diverse, depending upon the absence or presence of ssDNA, annealed DNA, or other causes of variation. Consequently, the proposed functional relationships may be superficial. The biochemical similarities may also be superficial. Rad52 and Redβ bind ssDNA weakly; however, they do so with significantly greater affinity compared to their binding of dsDNA. Both proteins anneal into a stable protein–DNA annealing intermediate when a complementary ssDNA is added to an existing protein–ssDNA complex.[17,18,27,28] These biochemical and structural similarities of Rad52 and Redβ could indicate a common genetic origin or just commonalities of appearance due to similar functions.

To elucidate the mechanism of strand annealing by Redβ and other SSAPs, we report here the outcome of two lines of research. First, we examined Redβ in various configurations by atomic force microscopy (AFM),[29] which allows imaging in physiological relevant conditions.[30–34] Complemented by biochemical and functional assays, we describe a new model for Redβ action. Second, using deep bioinformatic analysis, we discovered that the DNA binding domains of RecT/Redβ and Rad52 families are related. Hence, our model could define a commonality in SSAP action, including Rad52.

Results

Redβ complexes in the absence and presence of DNA

Redβ forms an unstable complex with ssDNA and a stable complex when annealing two complementary ssDNAs.[17,35] We assessed DNA annealing by Redβ in a band shift assay (Supplementary Fig. S1). The smeared bands characterizing Redβ–ssDNA binding indicate a low binding strength. However, upon annealing of two complementary ssDNAs, we observed a discrete band, which reflects a stable Redβ–dsDNA complex. These band shift results concord with the known DNA binding properties of Redβ. Redβ quaternary structures formed in the absence of DNA, in the presence of ssDNA, and upon the annealing of complementary ssDNAs were examined by high-resolution AFM (Supplementary Fig. S1). The three conformations of Redβ quaternary structure and Redβ–DNA complexes differed considerably.

Redβ alone forms a shallow right-handed helix

In the absence of DNA and without fixation, we observed the 11 or 12 subunit rings previously

observed by EM.[19] However, at higher resolution (Fig. 1), we could see that more than two-thirds of the AFM topographs (71%; $n = 184$) were not rings but gapped ellipses (Fig. 1b). A cross-correlation average of 668 structures, which included the 29% where the resolution was insufficient to see a gap (Fig. 1c), confirmed the slightly elliptical parameters; $a = 7.7 \pm 0.5$ nm and $b = 6.6 \pm 0.6$ nm with an eccentricity of 0.5 ± 0.5 (average of three independent measurements of the single cross correlation, Fig. 1d). The topographic profile of the average showed an increasing right-handed slope (Fig. 1e). However, the shallowness of the helix caused a steric clash at its ends, which presumably inhibited the addition of further Redβ monomers. Hence, we observed that Redβ forms a shallow helix similar to a split lock washer (Fig. 1i). Assuming a protein density of 1.42 g/cm³,[36] a Redβ monomer would give a spherical volume of 36.1 nm³ with a diameter of 4.1 nm. Without any overlap, 11 spherical Redβ monomers fit into the average (Fig. 1g). Allowing for a slight overlap, 12 Redβ monomers can be fitted into one helical turn (Fig. 1h). The height of the helix-forming Redβ monomer being in closest contact with the supporting surface was determined to be 3.5 ± 0.3 nm (Fig. 1f). This height is ≈15% smaller than would be predicted for a Redβ monomer adopting a spherical shape.

Redβ forms heterogeneous structures in the presence of ssDNA

The structures formed by Redβ binding to a 140-nt ssDNA were diverse, with little evidence of uni-formity or cooperative binding. In particular, no regularity was observed (Figs. 2 and Supplementary Fig. S1). However, monomeric structures could be distinguished in isolated Redβ–ssDNA complexes. The number of Redβ monomers per complex linearly correlated with the complex surface area up to a maximum of ≈11 Redβ monomers (Fig. 2c). We found one image where we could identify 23 apparent monomers and an equivalent surface area. This presumably represented two adjacent, fully bound Redβ–ssDNA complexes. The height of the Redβ–ssDNA complex of 2.6 ± 0.3 nm (Fig. 2d) was about one-fourth less than the Redβ monomer height observed in the absence of DNA (Fig. 1f) and about one-third less than that expected for a Redβ monomer adopting a spherical shape. This suggests that Redβ may adopt an elongated conformation in Redβ–ssDNA complexes. In selected cases, we could measure monomeric distances of 9.9 ± 2.1 nm along the apparent complex axis (Fig. 2b and e). Thus, compared to the observed regularity in the absence of DNA (above) or the presence of annealed DNA (below), the Redβ–ssDNA complex shows a considerable structural flexibility.

Redβ forms a pronounced left-handed helix upon annealing of complementary ssDNAs

Using conditions where Redβ promotes the annealing of complementary ssDNAs, AFM topographs were generated for DNA lengths of 83, 123, and 163 bp (Fig. 3). Regular-shaped Redβ–dsDNA complexes were observed, showing an average radius of 8.7 ± 1.2 nm that was independent from the DNA
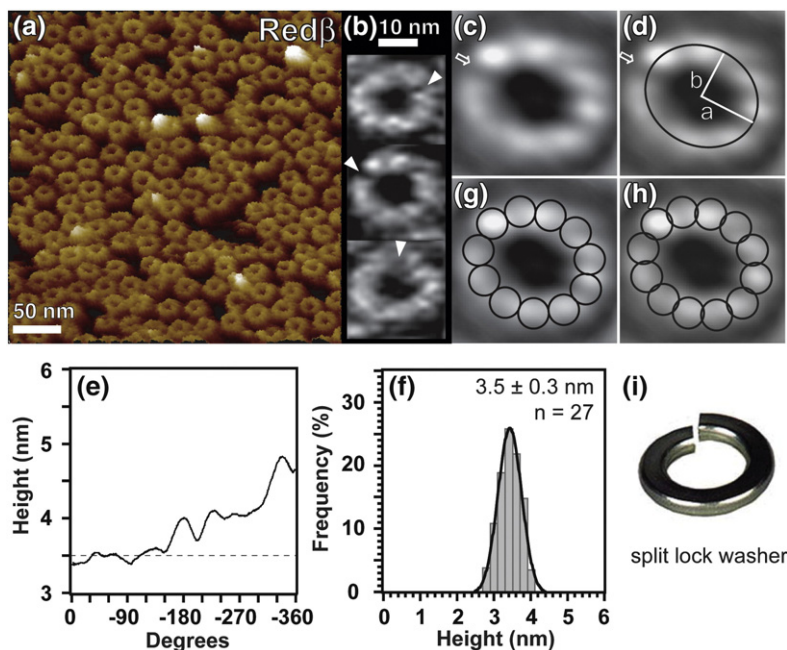

Fig. 1. Redβ polymer forms a shallow right-handed helical turn. (a) AFM topograph of Redβ polymers in the absence of DNA. (b) Gallery of single Redβ polymers imaged at high resolution. White arrows indicate an apparent structural clash between the lower (darker) and the higher (lighter) end of the Redβ polymer. (c) Cross-correlation average of 668 individual Redβ polymers. (d) A fitted ellipse along the highest points of the cross-correlation average in (c). (e) Height profile along the elliptical line, measured in counter-clockwise direction, represented as an amplitude envelope connecting the amplitude maxima, shows a shallow right-handed helicity of the Redβ polymer. Zero degrees correspond to white arrow in (d), and the broken line represents the average minimum height. (f) Average minimum heights measured at the lower end of the Redβ polymer. Data are presented as mean±SD. (g) Eleven Redβ monomers marked onto the cross-correlation average, assuming a Redβ monomer diameter of 4.1 nm and no overlapping. (h) Twelve Redβ monomers marked onto the cross-correlation average, assuming a Redβ monomer diameter of 4.1 nm and a slight overlapping between Redβ monomers. (i) In the absence of DNA, the quaternary structure of Redβ resembles a split lock washer.
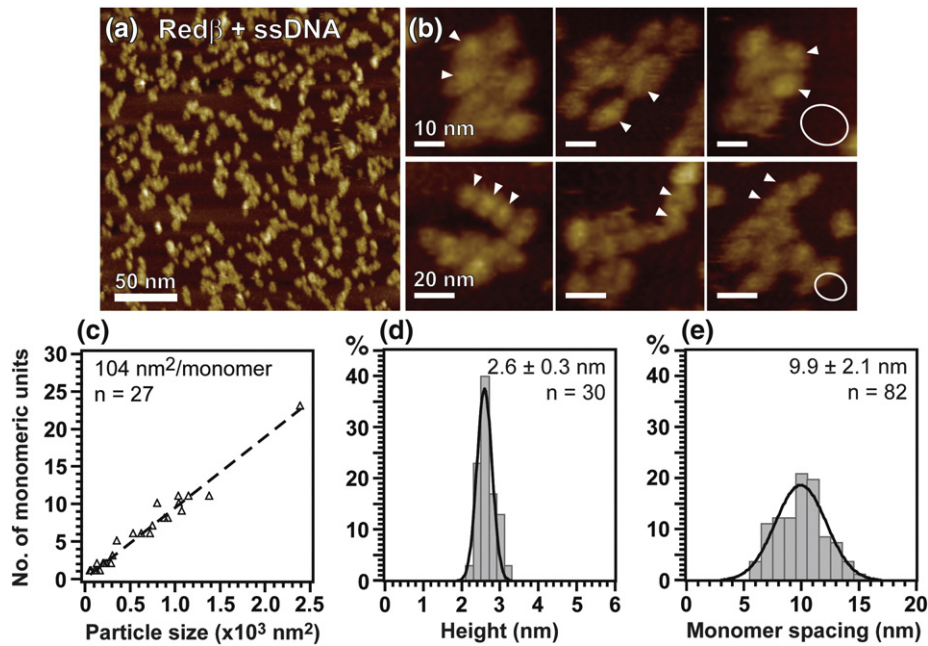
Fig. 2. Redβ forms heterogeneously shaped and disordered complexes in the presence of ssDNA. (a) AFM topographs of Redβ–ssDNA complexes obtained with 140 nt ssDNA. (b) Galleries of individual Redβ–ssDNA complexes display structural variations in shape and size. White arrowheads indicate sample complexes used to measure the peak-to-peak distance, and white circles indicate the size of the helical Redβ–ssDNA complex in Fig. 1g. (c) Number of monomeric units per complex (open triangles) as counted by eye and plotted against the respective complex surface area. The broken line represents a linear fit ($R^2 = 0.97$). (d) Height of the Redβ–ssDNA complex. (e) Distances between neighboring protrusions within the Redβ–ssDNA complexes (white arrowheads). Data are presented as mean±SD.

length (Fig. 3e). The contour length of these Redβ–dsDNA complexes increased linearly with the DNA length (Fig. 3f and g) with one exception. At DNA lengths of 163 bp, some complexes showed ringlike appearances, which can be explained by clash, or overlap of the ends of the helical Redβ–dsDNA complex. Thus, these ringlike complexes did not allow estimating the correct contour length (Fig. 3c and d). However, several 163-bp Redβ–dsDNA complexes appeared as S-shaped structures with no overlapping ends. Their contour length of 60.3± 3.0 nm ($n=10$) was in agreement with the linear relationship between DNA length and contour length of the Redβ–dsDNA complex (Fig. 3g). The S-shape suggests that the Redβ–dsDNA complex has been bent over by 180° and indicates a high structural flexibility. Based on a linear regression, the contour length of the Redβ–dsDNA complex increased by 0.36±0.03 nm/bp (Fig. 3g).

Every Redβ–dsDNA complex showed one lower (darker) and one higher (brighter) protruding end. In contrast to the shallow right-handed helix formed by Redβ alone (Fig. 1), the annealed Redβ–dsDNA structure resembles a pronounced left-handed helix (Fig. 4a). The height of the lowest end of the Redβ–dsDNA helix was 4.3±0.4 nm (Fig. 4b), which is 0.8 nm more than measured for a Redβ monomer in the absence of DNA (Fig. 1f) and suggests that the annealed DNA partially buries into the protein. High-resolution AFM topographs

(Fig. 4c) revealed the lateral distance between helical subunits as 4.0±0.8 nm (Fig. 4e). This distance correlated well with the diameter roughly approximated for the Redβ monomer (above). Thus, we suggest that each protrusion (Fig. 4d) corresponds to a Redβ monomer complexed with the annealed dsDNA.

Calculated parameters

Using the above measurements, we calculated the contour path length of one helical turn based on the average radii of 8.7 nm (Fig. 3e) and a pitch of 12.5 nm[19] to be 56 nm [given by $(2\pi*8.7)^2 + 12.5^2)^{0.5}$]. Using the average diameter of 4.0 nm per Redβ monomer (Fig. 4e), we estimate ≈14 Redβ monomers per helical turn. Thus, the Redβ–dsDNA complex encompasses between two and three Redβ monomers more per helical turn than the shallow right-handed Redβ helix in the absence of DNA. Thus, DNA annealing changes handedness and curvature of the Redβ helix. Based on the contour length increase of 0.36 nm/bp (Fig. 3g) and a protein path length of 56 nm, we calculate the binding of ≈155 bp DNA per helical turn. Because one helical turn consists of ≈14 Redβ monomers, this value reflects the binding of ≈11 bp DNA per Redβ monomer. All measured and calculated parameters are summarized in Table 1.
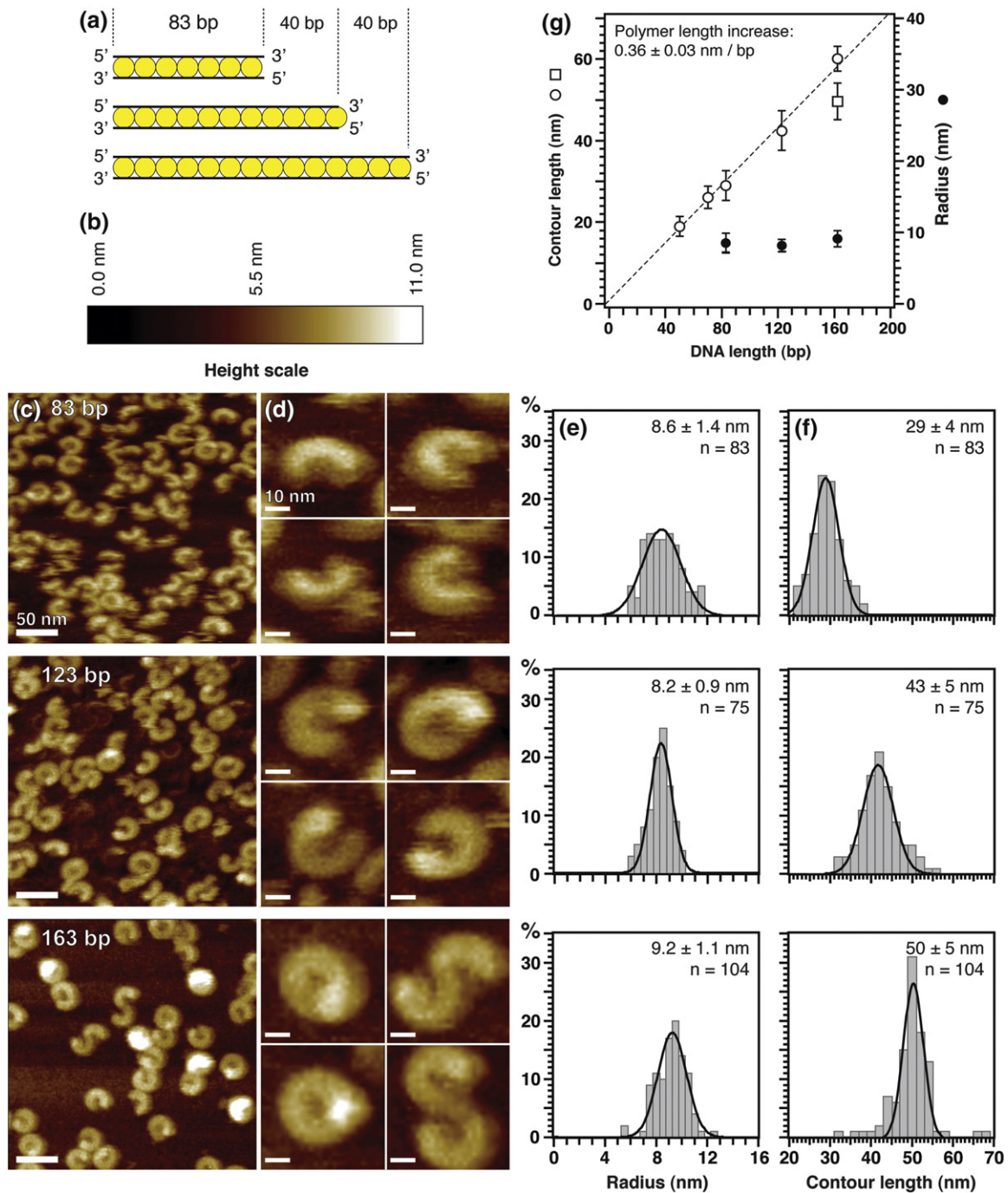
Fig. 3. Upon DNA annealing, Redβ forms a stable left-handed helix. (a) Schematic illustration of expected Redβ– dsDNA complexes. (b) Color code, scaling the vertical range of the AFM topographs. (c) AFM topographs of helical annealing intermediates obtained with 83-, 123-, and 163-bp-long DNA. (d) Galleries of individual Redβ–dsDNA complexes after annealing. (e) Histograms of the average helical radius of the helical annealing intermediate. (f) Histograms of the helical contour lengths. All histograms were fitted using Gaussian functions (continuous lines). Data are presented as mean±SD. (g) Contour lengths (empty circles) and radii (filled circles) of helical Redβ–dsDNA complexes plotted against DNA lengths. Redβ–dsDNA complex contour lengths for 83, 123, and 163 bp are based on (f); lengths for 50 and 70 bp were derived from AFM topographs shown in Supplementary Fig. S2. The broken line represents a linear fit to the helical contour length of the Redβ–dsDNA complex ($R^2 = 0.99$). The data point at 163 bp (empty circle) shows the average length of the S-shaped structures only (d), whereas the data point represented by the empty square shows the average length of all 163-bp structures.
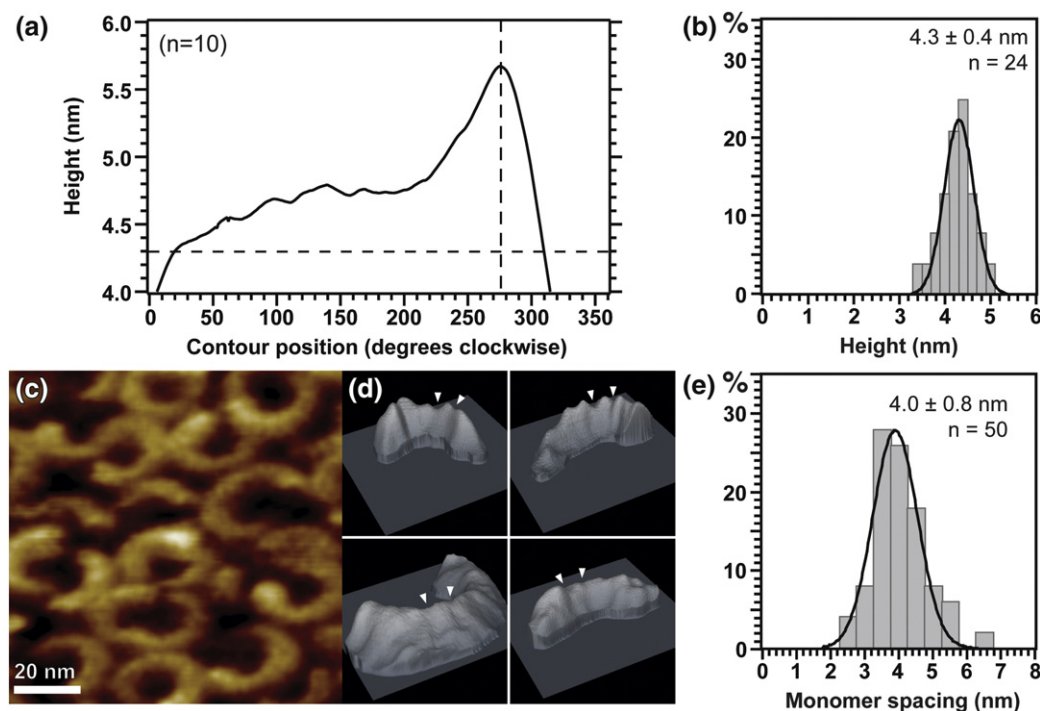
Fig. 4. Structural parameters of the Redβ annealing intermediate. (a) Average height profiles contouring helical Redβ–dsDNA complexes progressing in a clockwise orientation along the complex aligned at the maximum height (vertical broken line). The average was generated based on DNA–protein complexes observed for the 123-bp annealing experiment (Fig. 3d). The horizontal broken line shows the average of the lowest measured height of the complex. (b) The average lowest height of Redβ–dsDNA complexes was measured at the lower end of the helical complexes being in closest contact with the supporting mica surface. (c) High-resolution AFM topograph of helical Redβ–dsDNA complexes obtained with 123 bp annealed DNA. (d) Surface plots of helical sections displayed on a gray ground-level square of 29.3 nm×29.3 nm with a 2-fold stretch in z-scale. Full gray-level range corresponds to a vertical scale of 10 nm. White triangles indicate intersections between the protrusions. (e) Distribution of monomeric distances in the annealing intermediate. Data are presented as mean±SD.

The smallest possible stable annealing intermediate contains 16 to 20 bp DNA and a Redβ dimer

To further understand the substructure of the stable Redβ annealing intermediate, we examined the minimal DNA length required for Redβ annealing. By band shift, we found that stable complex formation requires more than 15 bp of complementary DNA sequence (Fig. 5a). To support the band shift experiment, we recorded AFM topographs of Redβ–dsDNA complexes containing 20- and 15-bp-long DNA (Fig. 5b). The AFM topographs showed that 20 bp DNA was sufficient to form the stable

Table 1. Summary of measured and calculated parameters of presented models

	Model A	Model B	Model C
	Redβ w/o DNA	Redβ–ssDNA	Annealed Redβ–DNA
Shape	Right-handed ellipse	Disordered	Left-handed helix
Radius (nm)[a]	7.1±0.4		8.7±1.2
Monomer/complex height (nm)[b]	3.5±0.3	2.6±0.3	4.3±0.4
Monomer spacing (nm)	4.1[c]	9.9±2.1	4.0±0.8
No. of Redβ monomers/turn	11±1		14±3
Path length/turn (nm)	45±4		56±4
Pitch (nm)	1.4±0.2		12.5[d]
DNA binding characteristics			
Bp/helix turn			155±18
Bp/Redβ monomer			11±3

[a] Measured at the highest protrusion of the Redβ monomer.
[b] Measured at the protein molecule exhibiting the lowest distance to the support.
[c] Predicted from theoretical volume calculations.
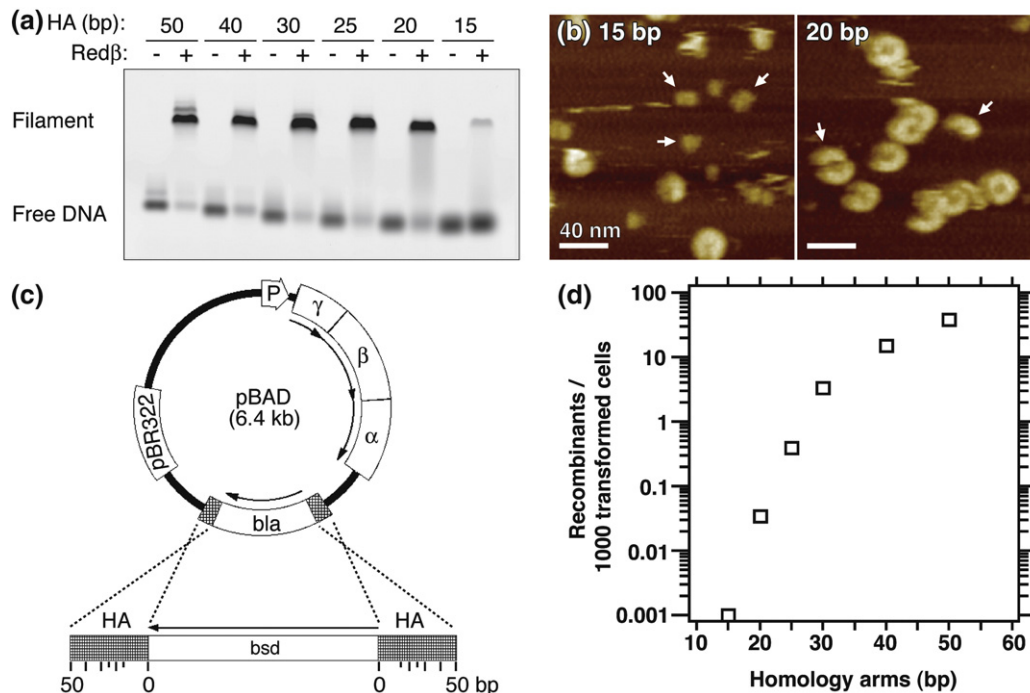[d] Taken from Ref. 19.

Fig. 5. Size of the smallest possible Redβ annealing intermediate. (a) Electrophoretic mobility shift assay showing complexes formed after incubation of Cy3-labeled, complementary oligonucleotides, from 15 to 50 bp, with or without Redβ as indicated. (b) AFM topographs of Redβ incubated with 15- or 20-bp-long complementary oligonucleotides. White arrows indicate monomeric Redβ molecules in the 15-bp image and dimers in the 20-bp image. Larger structures in the 20-bp image presumably indicate dimer aggregates. (c) Schematic illustration of the plasmid-based *in vivo* recombination assay. The diagram shows the pBAD plasmid with pBR322 ori, which expresses the Red operon (γ, β, α) from an L-arabinose-inducible promoter (P), and contains the ampicillin resistance gene (*bla*). Below, the ≈500-bp linear DNA molecule containing the blasticidin resistance gene (*bsd*) flanked by homology arms (HA), which varied in length up to 50 bp, is sketched. The homology arms were identical with sequences on either side of the ampicillin resistance gene, so that homologous recombination replaces *bla* with *bsd*, which can be easily scored by selection for the acquisition of blasticidin resistance and the loss of ampicillin resistance. (d) Homologous recombination efficiencies, measured as blasticidin-resistant colonies obtained per thousand transformed cells, using different homology arms from 15 to 50 bp.

annealing intermediate. In contrast, only a few helix-like structures surrounded by several dot-like structures, which approximately fit the dimension of a Redβ monomer, were observed when the DNA length was lowered to 15 bp. To test whether such small annealing intermediates are functionally relevant, we employed a plasmid-based assay for recombination in *Escherichia coli* (Fig. 5c). Using 50-bp-long homology arms, recombination occurred in 3.8% of all transformed cells. When 20-bp-long homology arms were used, a much lower efficiency of 0.034% was observed. However, the recombination efficiency with 15 bp homology arms was essentially zero, being at least 30 times less productive than 20 bp, whereas the difference between 20 and 25 bp was 10-fold (Fig. 5d). Consequently, these structural and functional observations suggest that the smallest possible and functionally active annealing intermediate must contain at least 16 to 20 bp of annealed dsDNA and two Redβ monomers.

Redβ–DNA complexes show 5′–3′ preference

After annealing, the DNA oligonucleotides used in Figs. 3, 4, and 5 produced dsDNA with blunt ends. To examine protruding single-stranded ends,

we employed oligonucleotides that annealed to give an 83-bp double-stranded region with 40-nt single-stranded tails on either the 5′ end or the 3′ end, or both ends. Measurements of the helix contour length identified two populations in the cases of one single-stranded end or three populations in the case of two overhangs (Supplementary Fig. S3). All measured lengths concord with the linear relationship plotted in Fig. 3g. Therefore, we conclude that the helical Redβ–dsDNA complex extends along the ssDNA overhangs. However, the helix extension from the annealed dsDNA region onto the ssDNA end showed a 5′–3′ preference. By comparing the peak areas, we estimate the preference for the 3′ ssDNA end to be 2.2-fold over the 5′ ssDNA end. These results show that the stable annealing intermediate can extend into the adjacent ssDNA with a 5′–3′ preference for stability.

Similarity of the RecT/Redβ and Rad52 families

Bioinformatic analysis defined that Redβ and Rad52 are members of two distinct SSAP families.[8] We reinvestigated this relationship by sensitive sequence searching and fold recognition. PSI-BLAST (position-specific iterated BLAST) searches using

various members of the Rad52 or RecT/Redβ family did not pick up members of the respective, other family. However, using the structure of the conserved N-terminal DNA binding domain of human Rad52, we tested the ability of RecT/Redβ and their homologs to adopt a similar fold to Rad52 by threading. Full-length Redβ and further related proteins of the RecT/Redβ family, as well as their DNA binding domains, identified the available structures of human Rad52 as highly significant hits. In contrast, no significant hits were detected when the same sequences were compared to the bacterial RecA, yeast, and/or human RAD51 atomic structures (Supplementary Fig. S3 and Table S1). These results led us to investigate the underlying sequence relationship in more detail. Multiple sequence alignments of the Rad52 and RecT/Redβ families revealed three conserved sequence motifs, which were used as anchoring points for the alignment, as shown in Fig. 7b. A few points of note emerge from the alignment. First, the overall architecture of the RecT/Redβ and Rad52 families is the same, based on the commonality of a conserved N-terminal DNA binding domain. Second, only the N-terminal parts of these proteins appear to be conserved to each other, as they have differing C-termini starting from approximately amino acid 175 (Fig. 7a). Third, the most highly conserved sequence motifs include the loop between α2 and β3, the end of β4, and end of α3 (Fig. 7b). Notably, these positively charged residues lie in the Rad52 groove, which is proposed to bind the phosphodiester backbone of ssDNA.[21] In particular, the conserved motif at the end of α3 includes residues that have been shown to be involved in DNA binding by human RAD52 (K152, R153, and R156) as well as Redβ (K148).[20,35] Based on these observations, we conclude that the ssDNA binding domains of the RecT/Redβ and Rad52 families are related.

Discussion

In homologous recombination, SSAPs such as Redβ and eukaryotic RAD52 promote the formation of joint molecules and second-end capture by DNA annealing.[28,37–39] To gain insight into the molecular mechanism, we examined Redβ quaternary structures without DNA, Redβ structures in complex with ssDNA, and Redβ structures after annealing in complex with dsDNA. Each of these complexes presented a different conformation. High-resolution AFM topographs of these conformations allowed us to develop a model for DNA annealing mediated by Redβ action. Based on the identification of structural homology and sequence similarity between the conserved N-terminal DNA binding domains of the RecT/Redβ and the RAD52 families, our model may present general structural and functional commonalities of SSAP DNA annealing mechanisms.

Redβ without DNA

Previous EM observations on Redβ in the absence of DNA reported oligomeric rings consisting of 11 or 12 Redβ monomers.[19] At low resolution, we also observed the same rings. However, at higher resolution, a shallow right-handed helix was observed, rather than a closed ring, indicating that Redβ monomers have an intrinsic ability to form a helical polymer not only after DNA annealing but also in the absence of DNA. Because closed rings are stable structures with ring completion often greatly contributing to the stability of an inherently unstable polymer,[40] the finding of an open helix explains why an apparently weak interaction with ssDNA is able to disassemble such a regular structure.

Redβ in complex with ssDNA

Redβ–ssDNA complexes were heterogeneous, as reflected by the weak binding to ssDNA in band shift gels. These observations concord with a lack of evidence for cooperative binding by Redβ to ssDNA.[17,18] As discussed for Rad52,[28] SSAPs may promote annealing by increasing the number of rapid transient encounters between individual protein-bound ssDNA molecules, rather than merely unraveling the intramolecular ssDNA secondary structure or blocking phosphodiester strand repulsion, which are properties also achieved by ssDNA binding proteins. Our observation that the Redβ polymer loses its regular shallow right-handed helical form, and binds monomerically to ssDNA, can be understood from this perspective. The observation that the minimum stable annealing intermediate contains only two Redβ monomers supports this model. The binding of ssDNA must be energetically more favorable than the gapped ring-binding mode. Hence, Redβ ssDNA binding could be driven by an increase of entropy.

Redβ in complex with annealed dsDNA

Upon annealing complementary ssDNA, a different helical complex is formed. Because the Redβ monomer spacing along the helical axis is the same in both the helix without DNA and the helix after annealing, we suggest that the two helices are essentially the same. However, there are two notable differences. First, the monomer within the helix is 0.8 nm higher after annealing than without DNA (Table 1). This increase can be explained by the binding of the DNA into a groove on the Redβ surface. Second, one helix is shallow and right-handed whereas the other is more pronounced and left-handed (Fig. 6). We suggest that the annealing of DNA and its tendency to turn into right-handed B-form drive this transition. If the annealed DNA remains bound to the protein and the two DNA strands do not cross each other with respect to the protein surface, then the left-handed helix would compensate for the right-handed torsion driven by the annealed DNA.

We show that Redβ-mediated DNA annealing requires only 16 to 20 bp of complementary DNA sequence and that the smallest possible annealing intermediate must contain two Redβ monomers,
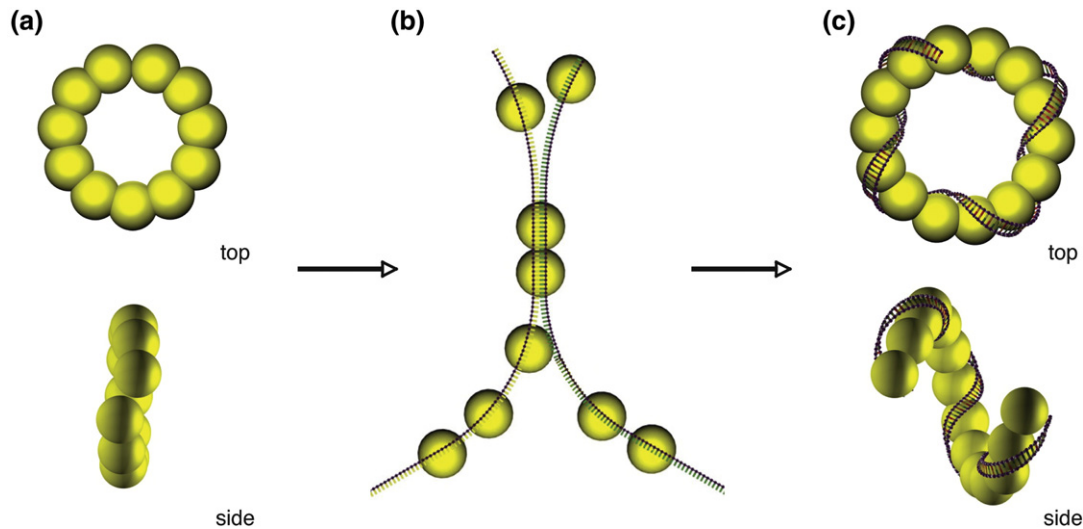
(a)   **(b)**   **(c)**

Fig. 6. Models of the Redβ quaternary structure in the absence of DNA, the disordered Redβ–ssDNA complex, and the Redβ–dsDNA complex after annealing. (a) Model of the right-handed helix of a Redβ polymer in the absence of DNA. (b) Model of the heterogeneous and disordered binding of Redβ to ssDNA and annealing initiation. (c) Model of the stable helical Redβ–dsDNA annealing intermediate, assuming that the bound DNA is stretched by a factor of 1.53 and takes a right-handed superhelical path around the left-handed Redβ helix. The two DNA strands do not cross each other with respect to the Redβ protein surface. Models were calculated according to experimental parameters given in Table 1.

which concords with recombineering practice. Usually, homology arm lengths as short as 35–50 bp are used,[13] corresponding to annealing intermediates, which contains only three to five Redβ monomers. The finding that Redβ is preferentially stable on 3′ single-stranded ends is in agreement with previous gel shift data.[41] The apparent 3′ preference for Redβ–DNA complexes accords with the fact that 3′ protruding single-stranded ends are generated by the cooperating 5′–3′ exonuclease, Redα. Furthermore, the 3′ end serves to prime DNA synthesis after annealing. Hence, a 5′–3′ directional preference may be a common mechanistic feature among SSAPs.

DNA path in the Redβ helix after annealing

We were able to measure three structural parameters: the helix height in the presence of annealed dsDNA (4.3 nm), the Redβ monomer spacing along the helical path of the protein (≈ 4.0 nm), and the number of nucleotides per Redβ monomer (≈ 11 bp) with a helix contour length extension of 0.36 nm/bp (Table 1). Although our topographs provide no direct evidence for the course of the DNA path along the protein helix, these values limit the number of possibilities. We consider two alternatives.

A Redβ monomer binds ≈ 11 bp, which is about one helical turn of B-form DNA. Hence, the first alternative is simply the binding of one B-form helical turn per Redβ monomer. To match B-form DNA and helix curvature, the DNA cannot be bound on the inside as previously proposed[19] but must be located along the middle radius of the protein helix. The second alternative is based on two rationales. First, DNA annealing initially requires an unwound double-stranded intermediate. Second, the two ssDNA

strands should not cross each other with respect to the protein surface. Both conditions are fulfilled if the two strands of DNA describe a superhelical 'train track' on the protein surface. Assuming that the annealed dsDNA is unwound by a factor of 1.53, as observed for RecA,[42] the DNA path length per helical turn is 80.5 nm, given by 155 bp × 0.52 nm/bp. We prefer a right-handed superhelical course, because it invokes right-handed base stacking and less negative supercoils than a left-handed course. Considering a helical pitch of 12.5 nm[19] and a Redβ circumference of 12.6 nm (4.0 nm diameter), the protein contour path length is 56.1 nm and the number of superhelix turns per protein helix turn is 4.6, given by $(80.5^2 - 56.1^2)^{0.5}/12.6$.

We cannot distinguish between the above two alternatives at present. The strength of the first lies in the regularity of binding one B-formed DNA double helix turn per Redβ molecule. On the other hand, it is known that Redβ does not bind to B-form DNA;[17] hence, the question 'why is the DNA not released from the protein?' arises. Furthermore, the 180° discontinuities observed in Fig. 3d are difficult to explain if the DNA shows the less-flexible B-form. The second alternative accommodates unwound DNA and presents several advantages. First, it would explain why the DNA is not released from the complex, and second, it suggests a reason for annealing catalysis via a stabilized unwound DNA intermediate. Releasing DNA from this stable intermediate possibly requires the action of DNA helicases.

Model for DNA annealing by Redβ

We propose a new model for Redβ-mediated DNA annealing (Fig. 6). Initially, random binding of ssDNA to Redβ disrupts the right-handed Redβ
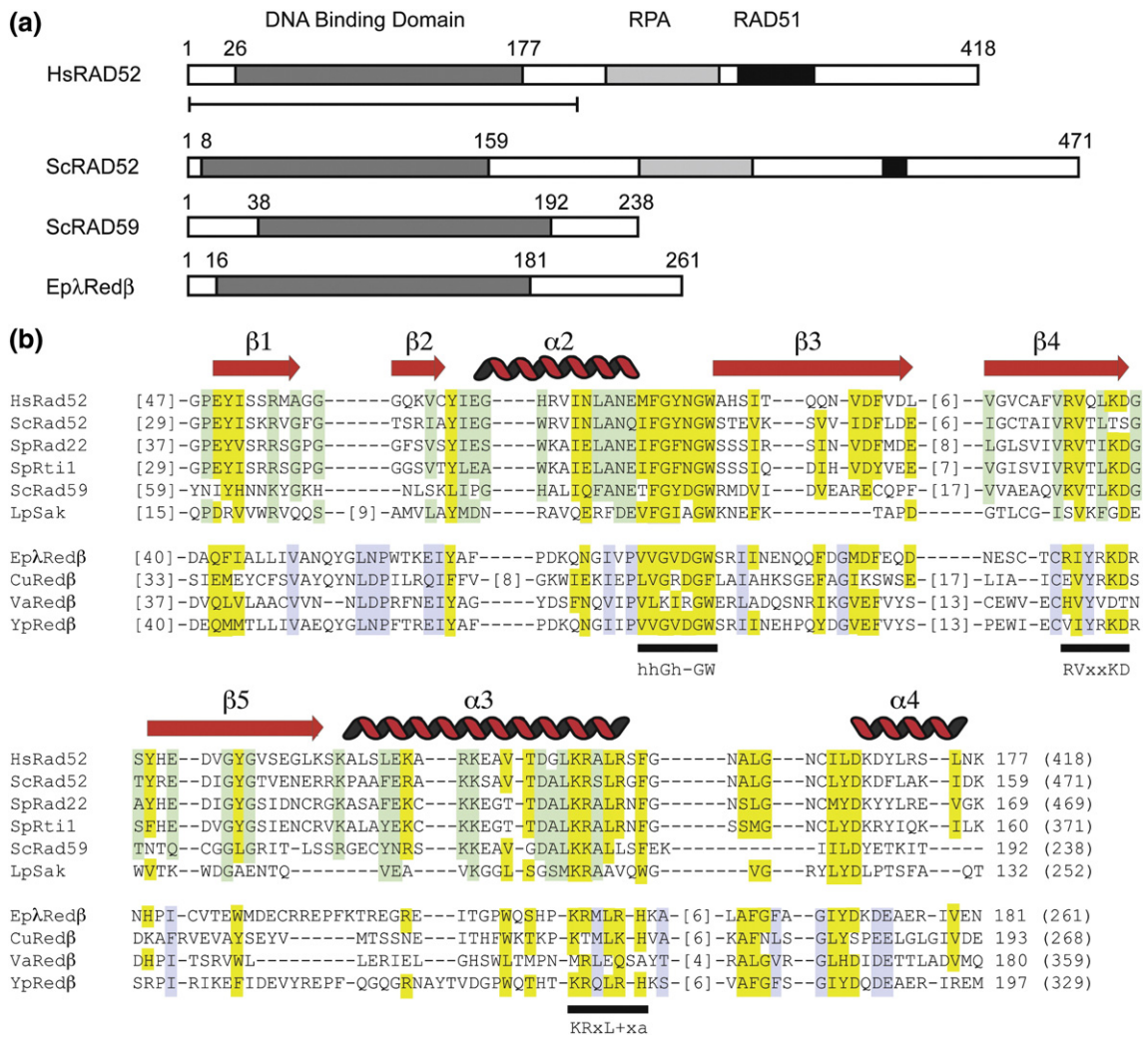
Fig. 7. Sequence similarity between the conserved DNA binding domains of Redβ and Rad52/Rad59 suggests a functional relationship in their DNA annealing mechanisms. (a) Schematic representation of the locations of the conserved DNA binding domain and the interaction motifs with RPA and RAD51 for human and yeast Rad52, yeast Rad59, and phage lambda Redβ. The black line underneath HsRAD52 depicts the region of its crystal structures.[20,21] (b) Multiple sequence alignment of the conserved N-terminal DNA binding domain of Rad52/Rad59 family members with representatives of the RecT/Redβ family.[8] Residues conserved between the Rad52 and RecT/Redβ families are highlighted in yellow, and family-specific conserved residues are highlighted in green and blue, respectively. Secondary structural elements indicated above the Rad52 family alignment were taken from the crystal structure of Rad52$_{1-212}$ (Protein Data Bank ID: 1KN0). Spirals and arrows indicate α-helices and β-strands, respectively, and were numbered according to previous assignments.[20] Numbers in brackets indicate residues in gaps not shown; the numbers in parentheses indicate the total sequence length. Sequence consensus below the alignment depicts conserved amino acid residues of particular motifs marked by a black line: hydrophobic (h), negatively charged (−), positively charged (+), polar (p), aromatic (a), any amino acid (x). Accession numbers and species abbreviations: Hs, *Homo sapiens*; Sc, *Saccharomyces cerevisiae*; Sp, *Schizosaccharomyces pombe*; Lp, *Lactococcus lactis* phage ul36; Epλ, Enterobacteria phage lambda; Cu, *Campylobacter upsaliensis* RM3195; Va, *Vibrio angustum* S14; Yp, *Yersinia pestis* biovar Orientalis; HsRad52, NP_602296; ScRad52, NP_013680; SpRad22, NP_593207; SpRti1, NP_595296; ScRad59, NP_010224; LpSak, NP_663647; EpλRedβ, NP_040617; CuRedβ, ZP_00372172; VaRedβ, ZP_01237386; VpRedβ, ZP_01174592.

helix and facilitates transient random interactions between ssDNAs. Upon the initiation of annealing, a second Redβ monomer binds to both the first Redβ monomer and the annealing DNA to form a stable complex. A stable annealing intermediate is formed, preferentially in the 5′–3′ direction, which adapts a left-handed superhelix due to the persistence of unwound dsDNA. Hence, Redβ facilitates both the discovery of local complementarities and then the propagation of annealing through polymerization. Whether this model applies for Rad52 or other SSAPs remains to be determined. However, our conclusion that Redβ does not form rings but a shallow helix, which is disrupted by ssDNA, not only offers a straightforward explanation for strand annealing catalysis but also may provoke a reevaluation of the rings formed by other SSAPs in the absence of DNA.

Similarities between Redβ and RAD52

Three distinct families of SSAPs have been defined based on sequence relationships.[8] Here, we present evidence that two of these families, Rad52 and RecT/Redβ, are structurally related. Not only do they share the similar architecture of their N-terminal, ≈155-aa ssDNA binding and annealing domain, but also we have been able to identify short regions of sequence similarity. Notably, these short regions are also the most conserved residues in the Rad52 family. Furthermore, the biochemical properties of Redβ and Rad52 are quite similar. Both proteins bind ssDNA with a greater affinity than dsDNA; however, ssDNA binding is weak.[17,27,28,35] Both proteins form stable annealing intermediates upon annealing, which apparently require action by further proteins to release dsDNA and both have been shown to mediate oligonucleotide-directed mutagenesis by DNA annealing *in vivo* with a strand-specific preference.[43–45] Both proteins can form (apparent) rings in the absence of DNA. While full-length human RAD52 forms a heptameric ring,[22] its N-terminal domain forms an undecameric ring similar to Redβ.[21] Recently, a quite similar model in terms of sampling and zipping was presented.[46] However, this model is based on the assumption that the physiological forms of RAD52 in complex with ssDNA are rings. Neither for Redβ nor for Rad52 is this assumption proven. Taken together, we propose that members of the Redβ/RecT and RAD52 families share structural and functional commonalities.

Materials and Methods

Sequence comparison of Redβ and Rad52 families and fold recognition

PSI-BLAST searches[47] were carried out against the non-redundant protein database using standard parameters and low-complexity filtering turned on. Multiple sequence alignments were done using ClustalX[48] with manual refinement. Sequences of the Redβ and Rad52 families were manually aligned using key features of sequence conservation within families as anchoring points. Fold recognition of representatives of each family that have associated functional information was done using the OpenProspect software (version of July 2007)[49] against the ASTRAL SCOP 1.71 database,[50] which includes all structures of the Protein Data Bank with less than 95% sequence similarity to each other. Fold recognition results were considered as being significant at a Z-score above 4.5 and were sorted according to their Z-scores, and the position of the Rad52 structures (1KN0[20] and 1H2I[21]) was noted in each hit list. To exclude the unordered C-terminal regions from threading and improve threading performance, we also submitted all sequences tested to the HMMerThread module of the ProFAT server[51] prior to OpenProspect, using an E-value cutoff for Hidden Markov Model-based domain detection of 50. This ensured that solely the RecT conserved domain (or any other domain of this family) was included in the threading run. Protein sequences shown in the multiple sequence alignment in Fig. 7b all scored with a significant Z-score and appeared

within the top 1.6% of the hit lists of both structural templates (1KN0 and 1H2I); in addition, they came up with a significant *p*-value (<0.05) in the HMMerThread-based threading runs.

Protein and DNA preparation and assays

Redβ full-length DNA sequence (accession code: NP_040617) was cloned into pASK-IBA2 expression vector, thereby a *Strep*-tag II was fused C-terminally. Recombinant protein was overexpressed in *E. coli* (GB2005; derivative of DH10B), affinity purified using a *Strep*-Tactin Superflow Sepharose column (IBA), and stored in 25 mM Tris–HCl, 50 mM NaCl, 0.1 mM ethylenediaminetetraacetic acid, and 20% glycerol, pH 8.0.

Oligonucleotides up to 140 nt were synthesized (biomers). Longer ssDNA was generated by PCR amplification and subsequent digestion by Redα (lambda exonuclease, NEB). Redβ–ssDNA complexes were generated by incubation for 40 min at 37 °C. Redβ–dsDNA complexes were generated by sequential addition of complementary ssDNAs and incubation at 37 °C for 40 min.[17] Redβ protein activity was tested employing an electrophoretic mobility shift assay using fluorescently labeled DNA and imaging buffer (see below). Redβ–DNA complexes were separated on 1.2% agarose gels. Fluorescent signals were recorded using either a Typhoon 9410 Variable Mode Imager (GE Healthcare). Recombineering was performed essentially as described using Redα, Redβ, Redγ, and a blasticidin cassette to replace the ampicillin resistance gene.[52]

AFM sample preparation and imaging

For AFM imaging of pure protein samples, Redβ protein was incubated at 1.4 μM for 10 min at 37 °C in B1 buffer (20 mM KH_2PO_4, pH 6.0, 10 mM MgCl_2, and 200 mM KCl). Afterwards, 25 μl of the sample was adsorbed on freshly cleaved mica for 30 min followed by extensive rinsing (3 times) with B1 buffer to remove non-adsorbed protein. Only for the high-resolution topographs in Fig. 1 was the adsorbed protein sample without DNA fixed to the mica surface by incubation with 0.2% (v/v) glutaraldehyde in B1 buffer for 2 min. All other topographs shown were acquired without any fixation procedures.

For all protein–DNA complex samples, 2.3 μM Redβ was first incubated in B2 buffer (20 mM KH_2PO_4, pH 6.0, and 10 mM MgCl_2) with either plus or minus ssDNA for 15 min at 37 °C to allow protein binding to the ssDNA. ssDNA concentrations were chosen to give a protein:DNA molar ratio of 1:4. For samples of Redβ with ssDNA, 20 μl of this incubation mix was taken for immediate adsorption on freshly cleaved mica (for details, see below). For samples of Redβ in complex with annealed dsDNA, an equimolar amount of the corresponding minus or plus ssDNA was added and the incubation mix was kept for an additional 40 min at 37 °C to allow for annealing. To yield a suitable complex density on the surface, we diluted samples before adsorption. Adsorption was allowed by placing 20 μl incubation mix for 10 min onto mica followed by rinsing (3 times) with buffer. Oscillation mode AFM imaging was performed with a Nanoscope III AFM (DI–Veeco) using Si_3N_4 cantilevers (OMCL TR-400 series, Olympus). Cantilevers were oscillated close to their resonance frequency, at amplitudes ranging between 1 and 5 nm. All height measurements were calibrated by simultaneous imaging of purple membrane patches from *Halobacterium salinarium* at height standard.[53]

Image processing and data analysis

Image processing of the topographs and height measurements were performed using standard procedures in the Nanoscope software version 5.12r2 (DI–Veeco). To reduce high frequency noise, we applied a low pass filter to high-resolution topographs of Figs. 1–3 and Supplementary Fig. S2. The average Redβ structure (Fig. 1) was achieved by correlation averaging of AFM topographs (512 × 512 pixels) performed with SEMPER image processing system.[54] One reference ring containing unit cell was selected from the raw data and cross-correlated with the topograph.[55] Afterwards, the unit cells were extracted according to the peak coordinates of the cross-correlated topograph. The single particle average was generated by translationally and rotationally aligning the 668 extracted unit cells to the reference ring.[56]

AFM topographs with a uniform height scaling of 10 nm were simplified into pictures giving the height information in black and white only in order to determine particle sizes. Redβ–DNA complex definition was done by a global cutoff of all information below 75% of the most prominent height of the complex. Afterwards, the size of each complex was determined by standard ImageJ version 1.37 analysis procedures. For the three-dimensional presentation of single protein–DNA complexes (Fig. 4d), high-resolution topographs were cut out from the raw data and processed using DINO [Visualizing Structural Biology (2002)†].

Contour lengths and radii of helical Redβ–dsDNA complexes (Fig. 3 and Supplementary Fig. S3) were determined semiautomatically by employing a DNA tracing routine in LabVIEW (National Instruments).[57,58] Refined models of Fig. 6 were generated employing computer-aided design supported by Quindium GmbH & Co. KG.

Supplementary Data

Supplementary data associated with this article can be found, in the online version, at doi:10.1016/j.jmb.2009.06.030

† http://www.dino3d.org

References

1. Cox, M. M., Goodman, M. F., Kreuzer, K. N., Sherratt, D. J., Sandler, S. J. & Marians, K. J. (2000). The importance of repairing stalled replication forks. *Nature*, **404**, 37–41.
2. McGlynn, P. & Lloyd, R. G. (2002). Recombinational repair and restart of damaged replication forks. *Nat. Rev., Mol. Cell. Biol.* **3**, 859–870.
3. van den Bosch, M., Lohman, P. H. & Pastink, A. (2002). DNA double-strand break repair by homologous recombination. *Biol. Chem.* **383**, 873–892.
4. Wyman, C. & Kanaar, R. (2004). Homologous recombination: down to the wire. *Curr. Biol.* **14**, R629–R631.
5. Kuzminov, A. (1999). Recombinational repair of DNA damage in *Escherichia coli* and bacteriophage lambda. *Microbiol. Mol. Biol. Rev.* **63**, 751–813.
6. Lin, Z., Kong, H., Nei, M. & Ma, H. (2006). Origins and evolution of the recA/RAD51 gene family: evidence for ancient gene duplication and endosymbiotic gene transfer. *Proc. Natl Acad. Sci. USA*, **103**, 10328–10333.
7. Cox, M. M. (2007). Motoring along with the bacterial RecA protein. *Nat. Rev., Mol. Cell. Biol.* **8**, 127–138.
8. Iyer, L. M., Koonin, E. V. & Aravind, L. (2002). Classification and evolutionary history of the single-strand annealing proteins, RecT, Redbeta, ERF and RAD52. *BMC Genomics*, **3**, 8.
9. Muyrers, J. P., Zhang, Y., Buchholz, F. & Stewart, A. F. (2000). RecE/RecT and Redalpha/Redbeta initiate double-stranded break repair by specifically interacting with their respective partners. *Genes Dev.* **14**, 1971–1982.
10. Kolodner, R., Hall, S. D. & Luisi-DeLuca, C. (1994). Homologous pairing proteins encoded by the *Escherichia coli* recE and recT genes. *Mol. Microbiol.* **11**, 23–30.
11. Court, D. L., Sawitzke, J. A. & Thomason, L. C. (2002). Genetic engineering using homologous recombination. *Annu. Rev. Genet.* **36**, 361–388.
12. Poteete, A. R. (2008). Involvement of DNA replication in phage lambda Red-mediated homologous recombination. *Mol. Microbiol.* **68**, 66–74.
13. Zhang, Y., Buchholz, F., Muyrers, J. P. & Stewart, A. F. (1998). A new logic for DNA engineering using recombination in *Escherichia coli*. *Nat. Genet.* **20**, 123–128.
14. Copeland, N. G., Jenkins, N. A. & Court, D. L. (2001). Recombineering: a powerful new tool for mouse functional genomics. *Nat. Rev., Genet.* **2**, 769–779.
15. Zhang, Y., Muyrers, J. P., Testa, G. & Stewart, A. F. (2000). DNA cloning by homologous recombination in *Escherichia coli*. *Nat. Biotechnol.* **18**, 1314–1317.
16. Muyrers, J. P., Zhang, Y., Testa, G. & Stewart, A. F. (1999). Rapid modification of bacterial artificial chromosomes by ET-recombination. *Nucleic Acids Res.* **27**, 1555–1557.
17. Karakousis, G., Ye, N., Li, Z., Chiu, S. K., Reddy, G. & Radding, C. M. (1998). The beta protein of phage lambda binds preferentially to an intermediate in DNA renaturation. *J. Mol. Biol.* **276**, 721–731.
18. Mythili, E., Kumar, K. A. & Muniyappa, K. (1996). Characterization of the DNA-binding domain of beta protein, a component of phage lambda red-pathway, by UV catalyzed cross-linking. *Gene*, **182**, 81–87.
19. Passy, S. I., Yu, X., Li, Z., Radding, C. M. & Egelman, E. H. (1999). Rings and filaments of beta protein from bacteriophage lambda suggest a super-family of recombination proteins. *Proc. Natl Acad. Sci. USA*, **96**, 4279–4284.

20. Kagawa, W., Kurumizaka, H., Ishitani, R., Fukai, S., Nureki, O., Shibata, T. & Yokoyama, S. (2002). Crystal structure of the homologous-pairing domain from the human Rad52 recombinase in the undecameric form. *Mol. Cell*, **10**, 359–371.

21. Singleton, M. R., Wentzell, L. M., Liu, Y., West, S. C. & Wigley, D. B. (2002). Structure of the single-strand annealing domain of human RAD52 protein. *Proc. Natl Acad. Sci. USA*, **99**, 13492–13497.

22. Stasiak, A. Z., Larquet, E., Stasiak, A., Müller, S., Engel, A., Van Dyck, E. *et al.* (2000). The human Rad52 protein exists as a heptameric ring. *Curr. Biol.* **10**, 337–340.

23. Van Dyck, E., Stasiak, A. Z., Stasiak, A. & West, S. C. (2001). Visualization of recombination intermediates produced by RAD52-mediated single-strand annealing. *EMBO Rep.* **2**, 905–909.

24. Ploquin, M., Bransi, A., Paquet, E. R., Stasiak, A., Yu, X., Cieslinska, A. M. *et al.* (2008). Functional and structural basis for a bacteriophage homolog of human RAD52. *Curr. Biol.* **18**, 1142–1146.

25. Thresher, R. J., Makhov, A. M., Hall, S. D., Kolodner, R. & Griffith, J. D. (1995). Electron microscopic visualization of RecT protein and its complexes with DNA. *J. Mol. Biol.* **254**, 364–371.

26. Poteete, A. R., Sauer, R. T. & Hendrix, R. W. (1983). Domain structure and quaternary organization of the bacteriophage P22 Erf protein. *J. Mol. Biol.* **171**, 401–418.

27. Kagawa, W., Kurumizaka, H., Ikawa, S., Yokoyama, S. & Shibata, T. (2001). Homologous pairing promoted by the human Rad52 protein. *J. Biol. Chem.* **276**, 35201–35208.

28. Mortensen, U. H., Bendixen, C., Sunjevaric, I. & Rothstein, R. (1996). DNA strand annealing is promoted by the yeast Rad52 protein. *Proc. Natl Acad. Sci. USA*, **93**, 10729–10734.

29. Binnig, G., Quate, C. F. & Gerber, C. (1986). Atomic force microscope. *Phys. Rev. Lett.* **56**, 930–933.

30. Shao, Z. & Zhang, Y. (1996). Biological cryo atomic force microscopy: a brief review. *Ultramicroscopy*, **66**, 141–152.

31. Muller, D. J., Sapra, K. T., Scheuring, S., Kedrov, A., Frederix, P. L., Fotiadis, D. & Engel, A. (2006). Single-molecule studies of membrane proteins. *Curr. Opin. Struct. Biol.* **16**, 489–495.

32. Lyubchenko, Y. L. (2004). DNA structure and dynamics: an atomic force microscopy study. *Cell Biochem. Biophys.* **41**, 75–98.

33. Hansma, H. G. (2001). Surface biology of DNA by atomic force microscopy. *Annu. Rev. Phys. Chem.* **52**, 71–92.

34. Engel, A. & Muller, D. J. (2000). Observing single biomolecules at work with the atomic force microscope. *Nat. Struct. Biol.* **7**, 715–718.

35. Wu, Z., Xing, X., Bohl, C. E., Wisler, J. W., Dalton, J. T. & Bell, C. E. (2006). Domain structure and DNA binding regions of beta protein from bacteriophage lambda. *J. Biol. Chem.* **281**, 25205–25214.

36. Fischer, H., Polikarpov, I. & Craievich, A. F. (2004). Average protein density is a molecular-weight-dependent function. *Protein Sci.* **13**, 2825–2828.

37. McIlwraith, M. J. & West, S. C. (2008). DNA repair synthesis facilitates RAD52-mediated second-end capture during DSB repair. *Mol. Cell*, **29**, 510–516.

38. Kmiec, E. & Holloman, W. K. (1981). Beta protein of bacteriophage lambda promotes renaturation of DNA. *J. Biol. Chem.* **256**, 12636–12639.

39. Muniyappa, K. & Radding, C. M. (1986). The homologous recombination system of phage lambda. Pairing activities of beta protein. *J. Biol. Chem.* **261**, 7472–7478.

40. Howard, J. (2001). *Mechanics of Motor Proteins and the Cytoskeleton.* Sinauer Associates, Inc., Sutherland, MA, 163.

41. Li, Z., Karakousis, G., Chiu, S. K., Reddy, G. & Radding, C. M. (1998). The beta protein of phage lambda promotes strand exchange. *J. Mol. Biol.* **276**, 733–744.

42. Stasiak, A., Di Capua, E. & Koller, T. (1981). Elongation of duplex DNA by recA protein. *J. Mol. Biol.* **151**, 557–564.

43. Ellis, H. M., Yu, D., DiTizio, T. & Court, D. L. (2001). High efficiency mutagenesis, repair, and engineering of chromosomal DNA using single-stranded oligonucleotides. *Proc. Natl Acad. Sci. USA*, **98**, 6742–6746.

44. Storici, F., Lewis, L. K. & Resnick, M. A. (2001). In vivo site-directed mutagenesis using oligonucleotides. *Nat. Biotechnol.* **19**, 773–776.

45. Zhang, Y., Muyrers, J. P., Rientjes, J. & Stewart, A. F. (2003). Phage annealing proteins promote oligonucleotide-directed mutagenesis in *Escherichia coli* and mouse ES cells. *BMC Mol. Biol.* **4**, 1.

46. Rothenberg, E., Grimme, J. M., Spies, M. & Ha, T. (2008). Human Rad52-mediated homology search and annealing occurs by continuous interactions between overlapping nucleoprotein complexes. *Proc. Natl Acad. Sci. USA*, **105**, 20274–20279.

47. Altschul, S. F., Madden, T. L., Schäffer, A. A., Zhang, J., Zhang, Z., Miller, W. & Lipman, D. J. (1997). Gapped BLAST and PSI-BLAST: a new generation of protein database search programs. *Nucleic Acids Res.* **25**, 3389–3402.

48. Larkin, M. A., Blackshields, G., Brown, N. P., Chenna, R., McGettigan, P. A., McWilliam, H. *et al.* (2007). Clustal W and Clustal X version 2.0. *Bioinformatics*, **23**, 2947–2948.

49. Kim, D., Xu, D., Guo, J. T., Ellrott, K. & Xu, Y. (2003). PROSPECT II: protein structure prediction program for genome-scale applications. *Protein Eng.* **16**, 641–650.

50. Murzin, A. G., Brenner, S. E., Hubbard, T. & Chothia, C. (1995). SCOP: a structural classification of proteins database for the investigation of sequences and structures. *J. Mol. Biol.* **247**, 536–540.

51. Bradshaw, C. R., Surendranath, V. & Habermann, B. (2006). ProFAT: a web-based tool for the functional annotation of protein sequences. *BMC Bioinformatics*, **7**, 466.

52. Wang, J., Sarov, M., Rientjes, J., Fu, J., Hollak, H., Kranz, H. *et al.* (2006). An improved recombineering approach by adding RecA to lambda Red recombination. *Mol. Biotechnol.* **32**, 43–53.

53. Heymann, J. B., Moller, C. & Muller, D. J. (2002). Sampling effects influence heights measured with atomic force microscopy. *J. Microsc.* **207**, 43–51.

54. Saxton, W. O., Pitt, T. J. & Horner, M. (1979). Digital image processing: the semper system. *Ultramicroscopy*, **4**, 343–353.

55. Saxton, W. O. & Baumeister, W. (1982). The correlation averaging of a regularly arranged bacterial cell envelope protein. *J. Microsc.* **127**, 127–138.

56. Saxton, W. O., Baumeister, W. & Hahn, M. (1984). Three-dimensional reconstruction of imperfect two-dimensional crystals. *Ultramicroscopy*, **13**, 57–70.

57. Wiggins, P. A., van der Heijden, T., Moreno-Herrero, F., Spakowitz, A., Phillips, R., Widom, J. *et al.* (2006). High flexibility of DNA on short length scales probed by atomic force microscopy. *Nat. Nanotechnol.* **1**, 137–141.

58. Moreno-Herrero, F., Seidel, R., Johnson, S. M., Fire, A. & Dekker, N. H. (2006). Structural analysis of hyperperiodic DNA from *Caenorhabditis elegans*. *Nucleic Acids Res.* **34**, 3057–3066.